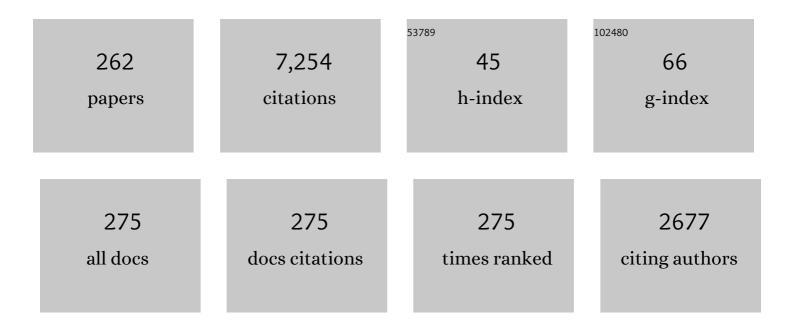
Libo Liu

List of Publications by Year in descending order

Source: https://exaly.com/author-pdf/369853/publications.pdf Version: 2024-02-01



Lieolui

#	Article	IF	CITATIONS
1	Solar activity variations of the ionospheric peak electron density. Journal of Geophysical Research, 2006, 111, .	3.3	193
2	ls an unusual large enhancement of ionospheric electron density linked with the 2008 great Wenchuan earthquake?. Journal of Geophysical Research, 2008, 113, .	3.3	175
3	Solar activity effects of the ionosphere: A brief review. Science Bulletin, 2011, 56, 1202-1211.	1.7	168
4	Wavenumberâ€4 patterns of the total electron content over the low latitude ionosphere. Geophysical Research Letters, 2008, 35, .	4.0	152
5	A brief review of equatorial ionization anomaly and ionospheric irregularities. Earth and Planetary Physics, 2018, 2, 1-19.	1.1	130
6	Variations of electron density based on long-term incoherent scatter radar and ionosonde measurements over Millstone Hill. Radio Science, 2005, 40, n/a-n/a.	1.6	127
7	A statistical analysis of ionospheric anomalies before 736 <i>M</i> 6.0+ earthquakes during 2002-2010. Journal of Geophysical Research, 2011, 116, n/a-n/a.	3.3	123
8	Climatology of the mean total electron content derived from GPS global ionospheric maps. Journal of Geophysical Research, 2009, 114, .	3.3	110
9	A study of the Weddell Sea Anomaly observed by FORMOSATâ€3/COSMIC. Journal of Geophysical Research, 2009, 114, .	3.3	105
10	Statistical analysis of solar activity variations of total electron content derived at Jet Propulsion Laboratory from GPS observations. Journal of Geophysical Research, 2009, 114, .	3.3	93
11	Seasonal variations of the ionospheric electron densities retrieved from Constellation Observing System for Meteorology, Ionosphere, and Climate mission radio occultation measurements. Journal of Geophysical Research, 2009, 114, .	3.3	91
12	Characteristics of the ionospheric total electron content of the equatorial ionization anomaly in the Asian-Australian region during 1996–2004. Annales Geophysicae, 2009, 27, 3861-3873.	1.6	81
13	An analysis of the scale heights in the lower topside ionosphere based on the Arecibo incoherent scatter radar measurements. Journal of Geophysical Research, 2007, 112, n/a-n/a.	3.3	78
14	A statistical study of largeâ€scale traveling ionospheric disturbances observed by GPS TEC during major magnetic storms over the years 2003–2005. Journal of Geophysical Research, 2008, 113, .	3.3	77
15	Topside ionospheric scale heights retrieved from Constellation Observing System for Meteorology, Ionosphere, and Climate radio occultation measurements. Journal of Geophysical Research, 2008, 113, .	3.3	73
16	Does the <i>F</i> _{10.7} index correctly describe solar EUV flux during the deep solar minimum of 2007-2009?. Journal of Geophysical Research, 2011, 116, n/a-n/a.	3.3	73
17	Observations and simulations of seismoionospheric GPS total electron content anomalies before the 12 January 2010 <i>M</i> 7 Haiti earthquake. Journal of Geophysical Research, 2011, 116, n/a-n/a.	3.3	73
18	Longitudinal variations of electron temperature and total ion density in the sunset equatorial topside ionosphere. Geophysical Research Letters, 2008, 35, .	4.0	72

#	Article	IF	CITATIONS
19	Features of the middle- and low-latitude ionosphere during solar minimum as revealed from COSMIC radio occultation measurements. Journal of Geophysical Research, 2011, 116, n/a-n/a.	3.3	72
20	A study on the nighttime midlatitude ionospheric trough. Journal of Geophysical Research, 2011, 116, .	3.3	70
21	Effects of solar variability on thermosphere density from CHAMP accelerometer data. Journal of Geophysical Research, 2007, 112, .	3.3	64
22	Latitudinal dependence of the ionospheric response to solar eclipses. Journal of Geophysical Research, 2009, 114, .	3.3	64
23	Statistical modeling of ionospheric foF2 over Wuhan. Radio Science, 2004, 39, n/a-n/a.	1.6	63
24	Effects of geomagnetic storm on GPS ionospheric scintillations at Sanya. Journal of Atmospheric and Solar-Terrestrial Physics, 2008, 70, 1034-1045.	1.6	61
25	The ionosphere under extremely prolonged low solar activity. Journal of Geophysical Research, 2011, 116, n/a-n/a.	3.3	61
26	Effects of disturbed electric fields in the lowâ€ l atitude and equatorial ionosphere during the 2015 St. Patrick's Day storm. Journal of Geophysical Research: Space Physics, 2016, 121, 9111-9126.	2.4	60
27	Yearly variations of global plasma densities in the topside ionosphere at middle and low latitudes. Journal of Geophysical Research, 2007, 112, .	3.3	59
28	Tidal wind mapping from observations of a meteor radar chain in December 2011. Journal of Geophysical Research: Space Physics, 2013, 118, 2321-2332.	2.4	58
29	Intraâ€annual variation of wave number 4 structure of vertical E × B drifts in the equatorial ionosphere seen from ROCSATâ€1. Journal of Geophysical Research, 2009, 114, .	3.3	57
30	Enhanced ionospheric plasma bubble generation in more active ITCZ. Geophysical Research Letters, 2016, 43, 2389-2395.	4.0	57
31	On the occurrence of postmidnight equatorial <i>F</i> region irregularities during the June solstice. Journal of Geophysical Research, 2011, 116, n/a-n/a.	3.3	56
32	Correlation between the ionospheric WN4 signature and the upper atmospheric DE3 tide. Journal of Geophysical Research, 2010, 115, .	3.3	54
33	Threeâ€dimensional lunar wake reconstructed from ARTEMIS data. Journal of Geophysical Research: Space Physics, 2014, 119, 5220-5243.	2.4	54
34	Anomalous enhancement of ionospheric electron content in the Asianâ€Australian region during a geomagnetically quiet day. Journal of Geophysical Research, 2008, 113, .	3.3	53
35	GPS TEC response to the 22 July 2009 total solar eclipse in East Asia. Journal of Geophysical Research, 2010, 115, .	3.3	52
36	Prestorm enhancements in Nm <i>F</i> ₂ and total electron content at low latitudes. Journal of Geophysical Research, 2008, 113, .	3.3	51

#	Article	IF	CITATIONS
37	A case study of postmidnight enhancement in Fâ€ŀayer electron density over Sanya of China. Journal of Geophysical Research: Space Physics, 2013, 118, 4640-4648.	2.4	51
38	Ionosphere disturbances observed throughout Southeast Asia of the superstorm of 20–22 November 2003. Journal of Geophysical Research, 2008, 113, .	3.3	50
39	Global scale annual and semi-annual variations of daytime NmF2 in the high solar activity years. Journal of Atmospheric and Solar-Terrestrial Physics, 2004, 66, 1691-1701.	1.6	49
40	Longâ€lasting negative ionospheric storm effects in low and middle latitudes during the recovery phase of the 17 March 2013 geomagnetic storm. Journal of Geophysical Research: Space Physics, 2016, 121, 9234-9249.	2.4	49
41	Modeling the global ionospheric total electron content with empirical orthogonal function analysis. Science China Technological Sciences, 2012, 55, 1161-1168.	4.0	48
42	The ionospheric anomalies prior to the M9.0 Tohoku-Oki earthquake. Journal of Asian Earth Sciences, 2013, 62, 476-484.	2.3	48
43	Solar activity variations of equivalent winds derived from global ionosonde data. Journal of Geophysical Research, 2004, 109, .	3.3	47
44	Applying artificial neural network to derive long-term foF2 trends in the Asia/Pacific sector from ionosonde observations. Journal of Geophysical Research, 2006, 111, .	3.3	47
45	Ionosphere around equinoxes during low solar activity. Journal of Geophysical Research, 2010, 115, .	3.3	46
46	Statistical analysis of ionospheric responses to solar flares in the solar cycle 23. Journal of Geophysical Research: Space Physics, 2013, 118, 576-582.	2.4	46
47	The GPS measured SITEC caused by the very intense solar flare on July 14, 2000. Advances in Space Research, 2005, 36, 2465-2469.	2.6	45
48	Planetary wave-type oscillations in the ionosphere and their relationship to mesospheric/lower thermospheric and geomagnetic disturbances at Wuhan (30.6°N, 114.5°E). Journal of Atmospheric and Solar-Terrestrial Physics, 2006, 68, 498-508.	1.6	45
49	Longitudinal characteristics of spread <i>F</i> backscatter plumes observed with the EAR and Sanya VHF radar in Southeast Asia. Journal of Geophysical Research: Space Physics, 2013, 118, 6544-6557.	2.4	45
50	Longitudinal development of lowâ€latitude ionospheric irregularities during the geomagnetic storms of July 2004. Journal of Geophysical Research, 2010, 115, .	3.3	44
51	Global characteristics of occurrence of an additional layer in the ionosphere observed by COSMIC/FORMOSAT-3. Geophysical Research Letters, 2011, 38, n/a-n/a.	4.0	44
52	Solar activity variations of nighttime ionospheric peak electron density. Journal of Geophysical Research, 2008, 113, .	3.3	43
53	Characterizing the 10 November 2004 stormâ€ŧime middleâ€ŀatitude plasma bubble event in Southeast Asia using multiâ€instrument observations. Journal of Geophysical Research, 2009, 114, .	3.3	43
54	Simulated wave number 4 structure in equatorial <i>F</i> â€region vertical plasma drifts. Journal of Geophysical Research, 2010, 115, .	3.3	42

#	Article	IF	CITATIONS
55	Equinoctial asymmetry of ionospheric vertical plasma drifts and its effect on <i>F</i> -region plasma density. Journal of Geophysical Research, 2011, 116, n/a-n/a.	3.3	42
56	A statistical study of ionospheric profile parameters derived from Millstone Hill incoherent scatter radar measurements. Geophysical Research Letters, 2004, 31, .	4.0	41
57	The midlatitude F2 layer during solar eclipses: Observations and modeling. Journal of Geophysical Research, 2008, 113, .	3.3	41
58	Modeling M(3000)F2 based on empirical orthogonal function analysis method. Radio Science, 2008, 43,	1.6	41
59	Coupling between mesosphere and ionosphere over Beijing through semidiurnal tides during the 2009 sudden stratospheric warming. Journal of Geophysical Research: Space Physics, 2013, 118, 2511-2521.	2.4	41
60	A prediction model of short-term ionospheric foF2 based on AdaBoost. Advances in Space Research, 2014, 53, 387-394.	2.6	41
61	Correlative study of plasma bubbles, evening equatorial ionization anomaly, and equatorial prereversal E Ā— B drifts at solar maximum. Radio Science, 2008, 43, .	1.6	40
62	Modeling the responses of the middle latitude ionosphere to solar flares. Journal of Atmospheric and Solar-Terrestrial Physics, 2007, 69, 1587-1598.	1.6	39
63	The propagation of traveling atmospheric disturbances observed during the April 6-7, 2000 ionospheric storm. Geophysical Research Letters, 2002, 29, 12-1-12-4.	4.0	37
64	Variability study of the crest-to-trough TEC ratio of the equatorial ionization anomaly around 120°E longitude. Advances in Space Research, 2009, 43, 1762-1769.	2.6	37
65	Statistical study of largeâ€scale traveling ionospheric disturbances generated by the solar terminator over China. Journal of Geophysical Research: Space Physics, 2013, 118, 4583-4593.	2.4	37
66	First results of the tidal structure in the MLT revealed by Wuhan Meteor Radar (30°40′N, 114°30′E). Journal of Atmospheric and Solar-Terrestrial Physics, 2004, 66, 675-682.	1.6	36
67	Equinoctial asymmetry in solar activity variations of <l>Nm</l> F2 and TEC. Annales Geophysicae, 2012, 30, 613-622.	1.6	36
68	The first time observations of low-latitude ionospheric irregularities by VHF radar in Hainan. Science China Technological Sciences, 2012, 55, 1189-1197.	4.0	36
69	Data assimilation of incoherent scatter radar observation into a oneâ€dimensional midlatitude ionospheric model by applying ensemble Kalman filter. Radio Science, 2007, 42, .	1.6	35
70	Solar activity dependence of the topside ionosphere at low latitudes. Journal of Geophysical Research, 2009, 114, .	3.3	35
71	Ionospheric total electron content variations prior to the 2008 Wenchuan Earthquake. International Journal of Remote Sensing, 2010, 31, 3545-3557.	2.9	35
72	A global morphology of gravity wave activity in the stratosphere revealed by the 8â€year SABER/TIMED data. Journal of Geophysical Research, 2012, 117, .	3.3	35

#	Article	IF	CITATIONS
73	GCITEM-IGGCAS: A new global coupled ionosphere–thermosphere-electrodynamics model. Journal of Atmospheric and Solar-Terrestrial Physics, 2009, 71, 2064-2076.	1.6	34
74	Longitudinal modulation of the O/N ₂ column density retrieved from TIMED/GUVI measurement. Geophysical Research Letters, 2010, 37, .	4.0	34
75	Further study on the solar activity variation of daytime <i>N_mF₂</i> . Journal of Geophysical Research, 2010, 115, .	3.3	34
76	A simulation study for the couplings between DE3 tide and longitudinal WN4 structure in the thermosphere and ionosphere. Journal of Atmospheric and Solar-Terrestrial Physics, 2012, 90-91, 52-60.	1.6	34
77	An update global model of hmF2 from values estimated from ionosonde and COSMIC/FORMOSAT-3 radio occultation. Advances in Space Research, 2014, 53, 395-402.	2.6	34
78	A case study of ionospheric storm effects during longâ€lasting southward IMF <i>B_z</i> â€driven geomagnetic storm. Journal of Geophysical Research: Space Physics, 2014, 119, 7716-7731.	2.4	34
79	Ionospheric response to the X-class solar flare on 7 September 2005. Journal of Geophysical Research, 2011, 116, n/a-n/a.	3.3	33
80	Seasonal behavior of equivalent winds over Wuhan derived from ionospheric data in 2000–2001. Advances in Space Research, 2003, 32, 1765-1770.	2.6	32
81	The low latitude ionospheric effects of the April 2000 magnetic storm near the longitude 120°E. Earth, Planets and Space, 2004, 56, 607-612.	2.5	32
82	Statistical analysis of ionospheric mid-latitude trough over the Northern Hemisphere derived from GPS total electron content data. Earth, Planets and Space, 2015, 67, .	2.5	32
83	Evaluation of global modeling of M(3000)F2 and hmF2 based on alternative empirical orthogonal function expansions. Advances in Space Research, 2010, 46, 1024-1031.	2.6	31
84	Development of a middle and low latitude theoretical ionospheric model and an observation system data assimilation experiment. Science Bulletin, 2008, 53, 94-101.	1.7	30
85	Strong evidence for couplings between the ionospheric wave-4 structure and atmospheric tides. Geophysical Research Letters, 2011, 38, n/a-n/a.	4.0	30
86	Highâ€speed stream impacts on the equatorial ionization anomaly region during the deep solar minimum year 2008. Journal of Geophysical Research, 2012, 117, .	3.3	30
87	Equatorial ionospheric electrodynamics during solar flares. Geophysical Research Letters, 2017, 44, 4558-4565.	4.0	30
88	Validation of COSMIC ionospheric peak parameters by the measurements of an ionosonde chain in China. Annales Geophysicae, 2014, 32, 1311-1319.	1.6	29
89	Modeling the behavior of ionosphere above Millstone Hill during the September 21–27, 1998 storm. Journal of Atmospheric and Solar-Terrestrial Physics, 2004, 66, 1093-1102.	1.6	27
90	The terdiurnal tide in the mesosphere and lower thermosphere over Wuhan (30°N, 114°E). Earth, Planets and Space, 2005, 57, 393-398.	2.5	27

#	Article	IF	CITATIONS
91	Influences of geomagnetic fields on longitudinal variations of vertical plasma drifts in the presunset equatorial topside ionosphere. Journal of Geophysical Research, 2009, 114, .	3.3	27
92	Statistical analysis of solar EUV and X-ray flux enhancements induced by solar flares and its implication to upper atmosphere. Journal of Geophysical Research, 2011, 116, n/a-n/a.	3.3	27
93	Simulated midlatitude summer nighttime anomaly in realistic geomagnetic fields. Journal of Geophysical Research, 2012, 117, .	3.3	27
94	Equatorial ionization anomaly in the lowâ€latitude topside ionosphere: Local time evolution and longitudinal difference. Journal of Geophysical Research: Space Physics, 2016, 121, 7166-7182.	2.4	27
95	Solar flare effects in the Earth's magnetosphere. Nature Physics, 2021, 17, 807-812.	16.7	27
96	Seasonal behavior of meteor radar winds over Wuhan. Earth, Planets and Space, 2005, 57, 61-70.	2.5	26
97	Global propagation features of large-scale traveling ionospheric disturbances during the magnetic storm of 7~10 November 2004. Annales Geophysicae, 2012, 30, 683-694.	1.6	26
98	Comparative study of the equatorial ionosphere over Jicamarca during recent two solar minima. Journal of Geophysical Research, 2012, 117, .	3.3	26
99	Variability of the behavior of the bottomside (B0, B1) parameters obtained from the ground-based ionograms at China's low latitude station. Advances in Space Research, 2008, 42, 695-702.	2.6	25
100	The discrepancy in solar EUVâ€proxy correlations on solar cycle and solar rotation timescales and its manifestation in the ionosphere. Journal of Geophysical Research, 2012, 117, .	3.3	25
101	Modeling study of nighttime enhancements in <i>F</i> region electron density at low latitudes. Journal of Geophysical Research: Space Physics, 2014, 119, 6648-6656.	2.4	25
102	Geomagnetic activity effect on the global ionosphere during the 2007–2009 deep solar minimum. Journal of Geophysical Research: Space Physics, 2014, 119, 3747-3754.	2.4	25
103	Comparison between ionospheric peak parameters retrieved from COSMIC measurement and ionosonde observation over Sanya. Advances in Space Research, 2014, 54, 929-938.	2.6	25
104	Comparative climatological study of largeâ€scale traveling ionospheric disturbances over North America and China in 2011–2012. Journal of Geophysical Research: Space Physics, 2014, 119, 519-529.	2.4	25
105	Seasonal variations of MLT tides revealed by a meteor radar chain based on Hough mode decomposition. Journal of Geophysical Research: Space Physics, 2015, 120, 7030-7048.	2.4	25
106	A study of the shape of topside electron density profile derived from incoherent scatter radar measurements over Arecibo and Millstone Hill. Radio Science, 2006, 41, n/a-n/a.	1.6	24
107	A comparative study of the bottomside profile parameters over Wuhan with IRI-2001 for 1999–2004. Earth, Planets and Space, 2006, 58, 601-605.	2.5	24
108	Automatic scaling of F2-layer parameters from ionograms based on the empirical orthogonal function (EOF) analysis of ionospheric electron density. Earth, Planets and Space, 2007, 59, 51-58.	2.5	24

#	Article	IF	CITATIONS
109	Modeling the effects of secular variation of geomagnetic field orientation on the ionospheric long term trend over the past century. Journal of Geophysical Research, 2008, 113, .	3.3	24
110	An analysis of thermospheric density response to solar flares during 2001–2006. Journal of Geophysical Research, 2012, 117, .	3.3	24
111	On the linkage of daytime 150 km echoes and abnormal intermediate layer traces over Sanya. Journal of Geophysical Research: Space Physics, 2013, 118, 7262-7267.	2.4	24
112	<i>N_mF₂</i> enhancement during ionospheric <i>F</i> ₂ region nighttime: A statistical analysis based on COSMIC observations during the 2007–2009 solar minimum. Journal of Geophysical Research: Space Physics, 2015, 120, 10083-10095.	2.4	24
113	Mapping the conjugate and corotating stormâ€enhanced density during 17 March 2013 storm through data assimilation. Journal of Geophysical Research: Space Physics, 2016, 121, 12,202.	2.4	24
114	lonospheric response to the geomagnetic storm on 13–17 April 2006 in the West Pacific region. Journal of Atmospheric and Solar-Terrestrial Physics, 2009, 71, 88-100.	1.6	23
115	Regional differences of the ionospheric response to the July 2012 geomagnetic storm. Journal of Geophysical Research: Space Physics, 2017, 122, 4654-4668.	2.4	23
116	The Storm Time Evolution of the Ionospheric Disturbance Plasma Drifts. Journal of Geophysical Research: Space Physics, 2017, 122, 11,665.	2.4	23
117	The variability of nonmigrating tides detected from TIMED/SABER observations. Journal of Geophysical Research: Space Physics, 2015, 120, 10,793.	2.4	22
118	The global distribution of the duskâ€ŧoâ€nighttime enhancement of summer <i>N_mF</i> ₂ at solar minimum. Journal of Geophysical Research: Space Physics, 2016, 121, 7914-7922.	2.4	22
119	The latitudinal structure of nighttime ionospheric TEC and its empirical orthogonal functions model over North American sector. Journal of Geophysical Research: Space Physics, 2017, 122, 963-977.	2.4	22
120	The 16-day waves in the mesosphere and lower thermosphere over Wuhan (30.6°N, 114.5°E) and Adelaide (35°S, 138°E). Advances in Space Research, 2005, 35, 2005-2010.	2.6	21
121	Statistical Study of the Storm Effects in Middle and Low Latitude Ionosphere in the Eastâ€Asian Sector. Chinese Journal of Geophysics, 2008, 51, 435-443.	0.2	21
122	Observations and modeling of the ionospheric behaviors over the east Asia zone during the 22 July 2009 solar eclipse. Journal of Geophysical Research, 2010, 115, .	3.3	21
123	Superposed epoch analyses of thermospheric response to CIRs: Solar cycle and seasonal dependencies. Journal of Geophysical Research, 2012, 117, .	3.3	21
124	The effect of solar radio bursts on the GNSS radio occultation signals. Journal of Geophysical Research: Space Physics, 2013, 118, 5906-5918.	2.4	21
125	The longâ€duration positive storm effects in the equatorial ionosphere over Jicamarca. Journal of Geophysical Research: Space Physics, 2015, 120, 1311-1324.	2.4	21
126	A global picture of ionospheric slab thickness derived from GIM TEC and COSMIC radio occultation observations. Journal of Geophysical Research: Space Physics, 2016, 121, 867-880.	2.4	21

#	Article	IF	CITATIONS
127	Mesospheric temperatures estimated from the meteor radar observations at Mohe, China. Journal of Geophysical Research: Space Physics, 2017, 122, 2249-2259.	2.4	21
128	Response of the topside ionosphere to recurrent geomagnetic activity. Journal of Geophysical Research, 2010, 115, .	3.3	20
129	The dawn enhancement of the equatorial ionospheric vertical plasma drift. Journal of Geophysical Research: Space Physics, 2015, 120, 10,688.	2.4	20
130	First observation of presunset ionospheric <i>F</i> region bottomâ€ŧype scattering layer. Journal of Geophysical Research: Space Physics, 2017, 122, 3788-3797.	2.4	20
131	Longitudinal behaviors of the IRI-B parameters of the equatorial electron density profiles retrieved from FORMOSAT-3/COSMIC radio occultation measurements. Advances in Space Research, 2010, 46, 1064-1069.	2.6	19
132	Formation of polar ionospheric tongue of ionization during minor geomagnetic disturbed conditions. Journal of Geophysical Research: Space Physics, 2015, 120, 6860-6873.	2.4	19
133	A TIEGCM numerical study of the source and evolution of ionospheric F-region tongues of ionization: Universal time and interplanetary magnetic field dependence. Journal of Atmospheric and Solar-Terrestrial Physics, 2017, 156, 87-96.	1.6	19
134	Two Day Wave Traveling Westward With Wave Number 1 During the Sudden Stratospheric Warming in January 2017. Journal of Geophysical Research: Space Physics, 2018, 123, 3005-3013.	2.4	19
135	El Niño–Southern Oscillation effect on quasi-biennial oscillations of temperature diurnal tides in the mesosphere and lower thermosphere. Earth, Planets and Space, 2018, 70, .	2.5	19
136	Equatorial Ionospheric Electrodynamics Over Jicamarca During the 6–11 September 2017 Space Weather Event. Journal of Geophysical Research: Space Physics, 2019, 124, 1292-1306.	2.4	19
137	Comparison of TEC from IRI-2016 and GPS during the low solar activity over Turkey. Astrophysics and Space Science, 2020, 365, 1.	1.4	19
138	Multiple Technique Observations of the Ionospheric Responses to the 21 June 2020 Solar Eclipse. Journal of Geophysical Research: Space Physics, 2020, 125, e2020JA028450.	2.4	19
139	Dipole tilt angle effect on magnetic reconnection locations on the magnetopause. Journal of Geophysical Research: Space Physics, 2015, 120, 5344-5354.	2.4	18
140	A modeling study of global ionospheric and thermospheric responses to extreme solar flare. Journal of Geophysical Research: Space Physics, 2016, 121, 832-840.	2.4	18
141	Largeâ€Scale Structure of Subauroral Polarization Streams During the Main Phase of a Severe Geomagnetic Storm. Journal of Geophysical Research: Space Physics, 2018, 123, 2964-2973.	2.4	18
142	Low latitude ionospheric effects near longitude 120°E during the great geomagnetic storm of july 2000. Science in China Series A: Mathematics, 2002, 45, 148-155.	0.5	17
143	Solar activity dependence of effective winds derived from ionospheric data at Wuhan. Advances in Space Research, 2003, 32, 1719-1724.	2.6	17
144	How does ionospheric TEC vary if solar EUV irradiance continuously decreases?. Earth, Planets and Space, 2014, 66, .	2.5	17

#	Article	IF	CITATIONS
145	Evidence and effects of the sunrise enhancement of the equatorial vertical plasma drift in the <i>F</i> region ionosphere. Journal of Geophysical Research: Space Physics, 2016, 121, 4826-4834.	2.4	17
146	Alfvén wings in the lunar wake: The role of pressure gradients. Journal of Geophysical Research: Space Physics, 2016, 121, 10,698.	2.4	17
147	Simulated longitudinal variations in the lower thermospheric nitric oxide induced by nonmigrating tides. Journal of Geophysical Research, 2011, 116, n/a-n/a.	3.3	16
148	Recent progress in ionospheric earthquake precursor study in China: A brief review. Journal of Asian Earth Sciences, 2015, 114, 420-430.	2.3	16
149	Statistical analysis of the mid-latitude trough position during different categories of magnetic storms and different storm intensities. Earth, Planets and Space, 2016, 68, .	2.5	16
150	Variations of the meteor echo heights at Beijing and Mohe, China. Journal of Geophysical Research: Space Physics, 2017, 122, 1117-1127.	2.4	16
151	Comparison of the observed topside ionospheric and plasmaspheric electron content derived from the COSMIC podTEC measurements with the IRI_Plas model results. Advances in Space Research, 2017, 60, 222-227.	2.6	16
152	An empirical model of ionospheric foE over Wuhan. Earth, Planets and Space, 2006, 58, 323-330.	2.5	15
153	Transition of Interhemispheric Asymmetry of Equatorial Ionization Anomaly During Solstices. Journal of Geophysical Research: Space Physics, 2018, 123, 10,283.	2.4	15
154	Persistence of the Longâ€Duration Daytime TEC Enhancements at Different Longitudinal Sectors During the August 2018 Geomagnetic Storm. Journal of Geophysical Research: Space Physics, 2020, 125, e2020JA028238.	2.4	15
155	Morphological Characteristics of Thousandâ€Kilometer‣cale E _s Structures Over China. Journal of Geophysical Research: Space Physics, 2021, 126, e2020JA028712.	2.4	15
156	Effects of the 21 June 2020 Solar Eclipse on Conjugate Hemispheres: A Modeling Study. Journal of Geophysical Research: Space Physics, 2020, 125, e2020JA028344.	2.4	14
157	Lithosphere ionosphere coupling associated with three earthquakes in Pakistan from GPS and GIM TEC. Journal of Geodynamics, 2021, 147, 101860.	1.6	14
158	Comparison of the first long-duration IS experiment measurements over Millstone Hill and EISCAT Svalbard radar with IRI2001. Advances in Space Research, 2006, 37, 1102-1107.	2.6	13
159	A theoretical model for mid- and low-latitude ionospheric electric fields in realistic geomagnetic fields. Science Bulletin, 2008, 53, 3883-3890.	9.0	13
160	Dusk-to-nighttime enhancement of mid-latitude <i>Nm</i> F2 in local summer: inter-hemispheric asymmetry and solar activity dependence. Annales Geophysicae, 2015, 33, 711-718.	1.6	13
161	Longitudinal Structure of the Midlatitude Ionosphere Using COSMIC Electron Density Profiles. Journal of Geophysical Research: Space Physics, 2018, 123, 8766-8777.	2.4	13
162	Unexpected High Occurrence of Daytime Fâ€Region Backscatter Plume Structures Over Low Latitude Sanya and Their Possible Origin. Geophysical Research Letters, 2020, 47, e2020GL090517.	4.0	13

#	Article	IF	CITATIONS
163	Deep-learning for ionogram automatic scaling. Advances in Space Research, 2020, 66, 942-950.	2.6	13
164	TIME3D-IGGCAS: A new three-dimension mid- and low-latitude theoretical ionospheric model in realistic geomagnetic fields. Journal of Atmospheric and Solar-Terrestrial Physics, 2012, 80, 258-266.	1.6	12
165	Modeling Chinese ionospheric layer parameters based on EOF analysis. Space Weather, 2015, 13, 339-355.	3.7	12
166	Nighttime electron density enhancements at middle and low latitudes in East Asia. Science China Earth Sciences, 2015, 58, 551-561.	5.2	12
167	New Features of the Enhancements in Electron Density at Low Latitudes. Journal of Geophysical Research: Space Physics, 2020, 125, e2019JA027539.	2.4	12
168	The Evolution of Equatorial Trough of Ionospheric F-region Ionization. Terrestrial, Atmospheric and Oceanic Sciences, 2001, 12, 559.	0.6	12
169	Model Study on Neutral Winds in the Ionospheric F- Region and Comparison with the Equivalent Winds Derived from the Wuhan Ionosonde Data. Terrestrial, Atmospheric and Oceanic Sciences, 2003, 14, 001.	0.6	12
170	A new method for determining the meridional wind velocity during an ionospheric storm. Geophysical Research Letters, 2003, 30, .	4.0	11
171	Lunar tidal winds in the mesosphere over Wuhan and Adelaide. Advances in Space Research, 2005, 36, 2218-2222.	2.6	11
172	Modeling the relationship between E × B vertical drift and the time rate of change of hmF2 (ΔhmF2/Δt) over the magnetic equator. Geophysical Research Letters, 2008, 35, .	4.0	11
173	Empirical modeling of ionospheric F2 layer critical frequency over Wakkanai under geomagnetic quiet and disturbed conditions. Science China Technological Sciences, 2012, 55, 1169-1177.	4.0	11
174	Discrepant responses of the global electron content to the solar cycle and solar rotation variations of EUV irradiance. Earth, Planets and Space, 2015, 67, .	2.5	11
175	GPS detection of the coseismic ionospheric disturbances following the 12 May 2008 M7.9 Wenchuan earthquake in China. Science China Earth Sciences, 2015, 58, 151-158.	5.2	11
176	Longâ€īerm Trend of Topside Ionospheric Electron Density Derived From DMSP Data During 1995–2017. Journal of Geophysical Research: Space Physics, 2019, 124, 10708-10727.	2.4	11
177	Prominent Daytime TEC Enhancements Under the Quiescent Condition of January 2017. Geophysical Research Letters, 2020, 47, e2020GL088398.	4.0	11
178	A Statistical Study on the Winter Ionospheric Nighttime Enhancement at Middle Latitudes in the Northern Hemisphere. Journal of Geophysical Research: Space Physics, 2020, 125, e2020JA027950.	2.4	11
179	Interhemispheric Transport of the Ionospheric <i>F</i> Region Plasma During the 2009 Sudden Stratosphere Warming. Geophysical Research Letters, 2020, 47, e2020GL087078.	4.0	11
180	Modeling the global ionospheric electron densities based on the EOF decomposition of the ionospheric radio occultation observation. Advances in Space Research, 2021, 68, 2218-2232.	2.6	11

#	Article	lF	CITATIONS
181	Deriving the effective scale height in the topside ionosphere based on ionosonde and satellite in situ observations. Journal of Geophysical Research: Space Physics, 2014, 119, 8472-8482.	2.4	10
182	An empirical model of the topside plasma density around 600 km based on ROCSATâ€1 and Hinotori observations. Journal of Geophysical Research: Space Physics, 2015, 120, 4052-4063.	2.4	10
183	A comparative study of GPS ionospheric scintillations and ionogram spread F over Sanya. Annales Geophysicae, 2015, 33, 1421-1430.	1.6	10
184	A comparison of mesospheric and lowâ€ŧhermospheric winds measured by Fabryâ€Perot interferometer and meteor radar over central China. Journal of Geophysical Research: Space Physics, 2016, 121, 10,037.	2.4	10
185	Statistical Behavior of the Longitudinal Variations of the Evening Topside Midâ€Latitude Trough Position in both Northern and Southern Hemispheres. Journal of Geophysical Research: Space Physics, 2018, 123, 3983-3997.	2.4	10
186	Statistics on the Magnetosheath Properties Related to Magnetopause Magnetic Reconnection. Astrophysical Journal, 2019, 880, 122.	4.5	10
187	Equatorial Northâ€South Difference of Noontime Electron Density Biteâ€Out in the <i>F</i> ₂ Layer. Journal of Geophysical Research: Space Physics, 2020, 125, e2020JA028124.	2.4	10
188	A Case Study of the Enhancements in Ionospheric Electron Density and Its Longitudinal Gradient at Chinese Low Latitudes. Journal of Geophysical Research: Space Physics, 2020, 125, e2019JA027751.	2.4	10
189	The sudden increase in ionospheric total electron content caused by the very intense solar flare on july 14, 2000. Science in China Series A: Mathematics, 2002, 45, 142-147.	0.5	9
190	Meteor radar observation of circulation near mesopause over Wuhan. Science Bulletin, 2003, 48, 1634-1638.	1.7	9
191	Observation of 6.5-day waves in the MLT region over Wuhan. Journal of Atmospheric and Solar-Terrestrial Physics, 2008, 70, 41-48.	1.6	9
192	Influence of DE3 tide on the equinoctial asymmetry of the zonal mean ionospheric electron density. Earth, Planets and Space, 2014, 66, 117.	2.5	9
193	αâ€Chapman Scale Height: Longitudinal Variation and Global Modeling. Journal of Geophysical Research: Space Physics, 2019, 124, 2083-2098.	2.4	9
194	Latitudinal Dependence of Daytime Electron Density Biteâ€Out in the Ionospheric F ₂ ‣ayer. Journal of Geophysical Research: Space Physics, 2021, 126, .	2.4	9
195	A Global Empirical Model of Electron Density Profile in the F Region Ionosphere Basing on COSMIC Measurements. Space Weather, 2021, 19, e2020SW002642.	3.7	9
196	Simulated longitudinal variations in the E-region plasma density induced by non-migrating tides. Journal of Atmospheric and Solar-Terrestrial Physics, 2012, 90-91, 68-76.	1.6	8
197	Modeling the global <i>Nm</i> F2 from the GNSSâ€derived TECâ€GIMs. Space Weather, 2013, 11, 272-283.	3.7	8
198	Global thermospheric disturbances induced by a solar flare: a modeling study. Earth, Planets and Space, 2015, 67, 3.	2.5	8

#	Article	IF	CITATIONS
199	Climatological modeling of horizontal winds in the mesosphere and lower thermosphere over a mid-latitude station in China. Advances in Space Research, 2015, 56, 1354-1365.	2.6	8
200	Peak height of OH airglow derived from simultaneous observations a Fabryâ€Perot interferometer and a meteor radar. Journal of Geophysical Research: Space Physics, 2017, 122, 4628-4637.	2.4	8
201	Responses of Solar Irradiance and the Ionosphere to an Intense Activity Region. Journal of Geophysical Research: Space Physics, 2018, 123, 2116-2126.	2.4	8
202	Trapped and Accelerated Electrons Within a Magnetic Mirror Behind a Flux Rope on the Magnetopause. Journal of Geophysical Research: Space Physics, 2019, 124, 3993-4008.	2.4	8
203	The Ionosphere at Middle and Low Latitudes Under Geomagnetic Quiet Time of December 2019. Journal of Geophysical Research: Space Physics, 2021, 126, e2020JA028964.	2.4	8
204	Unexpected Regional Zonal Structures in Low Latitude Ionosphere Call for a High Longitudinal Resolution of the Global Ionospheric Maps. Remote Sensing, 2022, 14, 2315.	4.0	8
205	Neutral wind-driven gradient drift instability in the low-latitude daytime <i>E</i> region. Journal of Geophysical Research, 2011, 116, .	3.3	7
206	On the relationship between the postmidnight thermospheric equatorial mass anomaly and equatorial ionization anomaly under geomagnetic quiet conditions. Journal of Geophysical Research, 2011, 116, n/a-n/a.	3.3	7
207	Simulated equinoctial asymmetry of the ionospheric vertical plasma drifts. Journal of Geophysical Research, 2012, 117, .	3.3	7
208	Shear in the zonal drifts of 3 m irregularities inside spread <i>F</i> plumes observed over Sanya. Journal of Geophysical Research: Space Physics, 2015, 120, 8146-8154.	2.4	7
209	New understanding achieved from 2 years of Chinese ionospheric investigations. Science Bulletin, 2016, 61, 524-542.	9.0	7
210	The effect of zonal wind reversal around sunset on ionospheric interhemispheric asymmetry at March equinox of a solar maximum year 2000. Journal of Geophysical Research: Space Physics, 2017, 122, 4726-4735.	2.4	7
211	Chinese ionospheric investigations in 2016–2017. Earth and Planetary Physics, 2018, , 89-111.	1.1	7
212	Variations of Thermospheric Winds Observed by a Fabry–Perot Interferometer at Mohe, China. Journal of Geophysical Research: Space Physics, 2021, 126, e2020JA028655.	2.4	7
213	Influence of interplanetary solar wind sector polarity on the ionosphere. Journal of Geophysical Research, 2012, 117, .	3.3	6
214	Equatorial Ionospheric Disturbance Fieldâ€Aligned Plasma Drifts Observed by C/NOFS. Journal of Geophysical Research: Space Physics, 2018, 123, 4192-4201.	2.4	6
215	New Aspects of the Ionospheric Behavior Over Millstone Hill During the 30â€Day Incoherent Scatter Radar Experiment in October 2002. Journal of Geophysical Research: Space Physics, 2019, 124, 6288-6295.	2.4	6
216	Evolution of the Subauroral Polarization Stream Oscillations During the Severe Geomagnetic Storm on 20 November 2003. Geophysical Research Letters, 2019, 46, 599-607.	4.0	6

#	Article	IF	CITATIONS
217	Recent ionospheric investigations in China (2018–2019). Earth and Planetary Physics, 2020, 4, 179-205.	1.1	6
218	Explaining Solar Flareâ€Induced Ionospheric Ion Upflow at Millstone Hill (42.6°N). Journal of Geophysical Research: Space Physics, 2022, 127, .	2.4	6
219	The effect of fluctuating ionospheric electric fields on Es-occurrence at cusp and polar cap latitudes. Advances in Space Research, 2001, 27, 1283-1288.	2.6	5
220	Gravity waves in the mesosphere observed with Wuhan meteor radar: A preliminary result. Advances in Space Research, 2003, 32, 831-836.	2.6	5
221	Modeling investigation of ionospheric storm effects over Millstone Hill during August 4–5, 1992. Earth, Planets and Space, 2004, 56, 903-908.	2.5	5
222	Dependence of thermospheric zonal winds on solar flux, geomagnetic activity, and hemisphere as measured by CHAMP. Journal of Geophysical Research: Space Physics, 2017, 122, 8893-8914.	2.4	5
223	An introduction to equatorial electrodynamics and a review of an additional layer at low latitudes. Journal of Atmospheric and Solar-Terrestrial Physics, 2018, 181, 94-109.	1.6	5
224	Longitudinal Differences in Electron Temperature on Both Sides of Zero Declination Line in the Midâ€latitude Topside Ionosphere. Journal of Geophysical Research: Space Physics, 2021, 126, e2020JA028471.	2.4	5
225	Occurrences of regional strong E s irregularities and corresponding scintillations characterized using a highâ€ŧemporalâ€ŧesolution GNSS network. Journal of Geophysical Research: Space Physics, 0, , .	2.4	5
226	Daytime Ionospheric Largeâ€Scale Plasma Density Depletion Structures Detected at Low Latitudes Under Relatively Quiet Geomagnetic Conditions. Journal of Geophysical Research: Space Physics, 2022, 127, .	2.4	5
227	Concurrent effects of Martian topography on the thermosphere and ionosphere at high northern latitudes. Earth, Planets and Space, 2022, 74, .	2.5	5
228	Responding trends of ionospheric <i>F</i> ₂ -layer to weaker geomagnetic activities. Journal of Space Weather and Space Climate, 2022, 12, 6.	3.3	5
229	A New Global Ionospheric Electron Density Model Based on Grid Modeling Method. Space Weather, 2022, 20, .	3.7	5
230	lonospheric precursors of strong earthquakes observed using six GNSS stations data during continuous five years (2011–2015). Geodesy and Geodynamics, 2023, 14, 65-79.	2.2	5
231	A simulation study on the semiannual variation of the ionosphericF2layer zonal electric fields at the magnetic equator. Journal of Geophysical Research, 2006, 111, .	3.3	4
232	TIME-IGGCAS model validation: Comparisons with empirical models and observations. Science in China Series D: Earth Sciences, 2008, 51, 308-322.	0.9	4
233	Global tidal mapping from observations of a radar campaign. Advances in Space Research, 2017, 60, 130-143.	2.6	4
234	Occurrence of Ionospheric Equatorial Ionization Anomaly at 840Âkm Height Observed by the DMSP Satellites at Solar Maximum Dusk. Space Weather, 2021, 19, e2020SW002690.	3.7	4

#	Article	IF	CITATIONS
235	Equinoctial Asymmetry in Solar Quiet Fields along the 120° E Meridian Chain. Applied Sciences (Switzerland), 2021, 11, 9150.	2.5	4
236	Simulated east–west differences in F-region peak electron density at Far East mid-latitude region. Earth, Planets and Space, 2020, 72, .	2.5	4
237	Ionospheric Nighttime Enhancements at Low Latitudes Challenge Performance of the Global Ionospheric Maps. Remote Sensing, 2022, 14, 1088.	4.0	4
238	Persistent Eastward EEJ Enhancement During the Geomagnetic Storm Recovery Phases. Journal of Geophysical Research: Space Physics, 2022, 127, .	2.4	4
239	Whistler Wings and Reflected Particles During Solar Wind Interaction of Lunar Magnetic Anomalies. Geophysical Research Letters, 2021, 48, e2021GL092425.	4.0	3
240	Measurement of Martian atmospheric winds by the O2 1.27 μm airglow observations using Doppler Michelson Interferometry: A concept study. Science China Earth Sciences, 2021, 64, 2027-2042.	5.2	3
241	Anomaly distribution of ionospheric total electron content responses to some solar flares. Earth and Planetary Physics, 2019, 3, 1-8.	1.1	3
242	A Meandering Lunar Wake Produced by the Pickup of Reflected Solarâ€Wind Ions. Geophysical Research Letters, 2021, 48, .	4.0	3
243	Theoretical Modeling and Analysis of Thermospheric Winds in the Ionosphere. Chinese Journal of Geophysics, 2003, 46, 1058-1067.	0.2	2
244	Seasonal variations of night mesopause temperature in Beijing observed by SATI4. Science China Technological Sciences, 2012, 55, 1295-1301.	4.0	2
245	Westward Electric Fields in the Afternoon Equatorial Ionosphere During Geomagnetically Quiet Times. Journal of Geophysical Research: Space Physics, 2020, 125, e2020JA028532.	2.4	2
246	ULF Fluctuation of Lowâ€Latitude Ionospheric Electric Fields During Sudden Commencements. Journal of Geophysical Research: Space Physics, 2022, 127, .	2.4	2
247	A 3D Empirical Model of Electron Density Based on CSES Radio Occultation Measurements. Space Weather, 2022, 20, .	3.7	2
248	Manifestation of planetary wave-type oscillations in variations in the critical frequencies of the ionospheric F2 layer in the Asian region. Geomagnetism and Aeronomy, 2011, 51, 762-773.	0.8	1
249	The Feature of Ionospheric Mid-Latitude Trough during Geomagnetic Storms Derived from GPS Total Electron Content (TEC) Data. Remote Sensing, 2022, 14, 369.	4.0	1
250	Paint to Better Describe: Learning Image Caption by Using Text-to-Image Synthesis. , 2021, , .		1
251	A New Method for Retrieving Electron Density Profiles from the MARSIS Ionograms. Remote Sensing, 2022, 14, 1817.	4.0	1
252	Comment on the paper "Total solar eclipse of July 22, 2009: Its impact on the total electron content and ionospheric electron density in the Indian zone―by Sharma et al Journal of Atmospheric and Solar-Terrestrial Physics, 2011, 73, 2034-2038.	1.6	0

#	Article	IF	CITATIONS
253	Structure and Dynamics of Ionospheric Plasma. International Journal of Geophysics, 2011, 2011, 1-2.	1.1	0
254	A simulation on the global mean structure of the ionosphere and thermosphere. , 2014, , .		0
255	Preface: Advances in equatorial, low- and mid-latitude mesosphere, thermosphere and ionosphere studies. Advances in Space Research, 2015, 56, 1805.	2.6	0
256	An ionospheric assimilation model along a meridian plane. Journal of Atmospheric and Solar-Terrestrial Physics, 2016, 145, 125-135.	1.6	0
257	The Highâ€Latitude Trough in the Southern Hemisphere Observed by Swarmâ€A Satellite. Journal of Geophysical Research: Space Physics, 2019, 124, 9475-9485.	2.4	0
258	Interhemispheric conjugate effect in longitude variations of mid-latitude ion density. Journal of Space Weather and Space Climate, 2019, 9, A40.	3.3	0
259	Meteor radar observation of circulation near mesopause over Wuhan. Science Bulletin, 2003, 48, 1634.	1.7	0
260	Numerical simulation of three dimensional flow in Yazidang Reservoir based on image processing. Journal of Intelligent and Fuzzy Systems, 2020, 39, 1591-1600.	1.4	0
261	Extreme Enhancements of Electron Temperature in Low Latitude Topside Ionosphere During the October 2016 Storm. Journal of Geophysical Research: Space Physics, 2022, 127, .	2.4	0
262	The north–south asymmetry of Martian ionosphere and thermosphere. Journal of Geophysical Research E: Planets, 0, , .	3.6	0